PAPER

Check for updates

In situ Raman and FTIR spectroscopic study on the formation of the isomers MIL-68(Al) and MIL-53(Al)†

Heidemarie Embrechts,[ab] Martin Kriesten, [ID][c] Matthias Ermer, [ID][c] Wolfgang Peukert, [ID][ab] Martin Hartmann [ID] *[bc] and Monica Distaso [ID] *[ab]

The topological metal–organic framework isomers MIL-53 and MIL-68 form from similar educts but differ in their pore geometries. They have been known for several years, but their synthesis is always reported separately. In consequence, the underlying mechanism and decisive synthesis parameters leading to the formation of either MIL-53 or MIL-68 are not understood. The present study shows how to induce the formation of MIL-68(Al) rather than MIL-53(Al) at low synthesis temperatures in *N,N*-dimethylformamide (DMF) using a modulated synthesis approach. MIL-68(Al) is identified as the intermediate product of formic acid modulated synthesis, which converts into the thermodynamically stable MIL-53(Al) product at longer synthesis times. The interactions of formic acid with the synthesis precursors responsible for inducing MIL-68(Al) formation are investigated with *in situ* Raman and FTIR spectroscopy. In contrast to the commonly assumed modulation mechanism of competitive coordination of linker and modulator with the metal node, formic acid is shown to form hydrogen bonds *via* the carboxylic group of the terephthalic acid (H_2BDC) linker, slowing prenucleation building unit and subsequent crystal growth. MIL-68(Al) formation is favored by the combination of a deficiency of terephthalic acid in solution and a slow MOF growth rate. Dissolved H_2BDC in solution is proposed to hinder MIL-68(Al) formation by serving as a molecular template for the rhombic MIL-53(Al) pore channels.

1. Introduction

Metal–organic frameworks (MOFs) have been the subject of intense research interest in the past two decades.[1] Their extremely high surface areas, highly-organized micropore networks, wide range of geometries, dynamic framework effects and ease of functionalization make them promising candidates for a variety of applications in the fields of gas adsorption, separation[2,3] and storage,[4,5] catalysis,[6,7] luminescence,[8] drug delivery[9,10] and sensing.[11] However, the underlying formation mechanism and effect of synthesis conditions on the resulting MOF structures are often not well understood.

Mechanistic understanding of the relationship between synthesis conditions and the resulting MOF polymorph

structures is necessary to rationally synthesize tailor-made MOFs for specific applications.[12] Gascon *et al.* demonstrated with *in situ* small-angle X-ray scattering (SAXS) and energy dispersive X-ray diffraction (EDXRD) the role of water in promoting the formation of the thermodynamically stable NH₂-MIL-53(Al) product rather than the kinetically favored NH₂-MOF-235(Al) and NH₂-MIL-101(Al) products formed in *N,N*-dimethylformamide (DMF) from amino-functionalized terephthalic acid ($H_2BDC-NH_2$) linker.[13–15] Haouas *et al.* demonstrated with *in situ* liquid-state ²⁷Al- and ¹H-NMR measurements that the formation pathways leading to the MIL-96, MIL-100 and MIL-110 Al trimesate structures are determined by the synthesis pH, which influences the preferential formation of various intermediate prenucleation building unit (PNBU) species.[16] The preferential formation of MIL-88B(V) rather than its framework isomer MIL-101(V) in the presence of HCl and the irreversible transformation of both structures into the thermodynamically stable MIL-47(V) product was investigated by Carson *et al.*[17] MOF isomers are assembled from the same secondary building units and organic linkers but have different framework structures.

In this study, *in situ* Raman and FTIR spectroscopy is used to gain understanding of the synthesis parameters and conditions to preferentially obtain the MIL-68(Al) structure rather than its more-studied framework isomer MIL-53(Al). MIL-68 and MIL-53

[a]*Institute of Particle Technology, FAU Erlangen-Nürnberg, Cauerstr. 4 – 91058, Erlangen, Germany. E-mail: monica.distaso@fau.de; heidemarie.embrechts@fau.de; wolfgang.peukert@fau.de*

[b]*Interdisciplinary Center for Functional Particle Systems, FAU Erlangen-Nürnberg, Haberstr. 9a – 91058, Erlangen, Germany*

[c]*Erlangen Center for Interface Research and Catalysis (ECRC), FAU Erlangen-Nürnberg, Egerlandstr. 3 – 91058, Erlangen, Germany. E-mail: martin.hartmann@ecrc.uni-erlangen.de; martin.kriesten@fau.de; matthias.ermer@fau.de*

are both composed of trans $MO_4(OH)_2$ octahedra chains, containing Fe, In, Ga, V or Al metal centers, connected by hydroxyl groups and terephthalate ligands. The MOFs are synthesized from similar educts, but differ in their network connectivity and properties. MIL-53 contains rhombic pore channels with a diameter of 8.5 Å in its large pore form,[18,19] while MIL-68 has a Kagomé topology containing both 6.0–6.4 Å triangular and 16–17 Å hexagonal channels.[20,21] The MIL-53 framework is flexible and undergoes a so-called "breathing" upon absorption of guest molecules.[18,22] MIL-68 is a rigid MOF, especially interesting for separation applications due to its two distinct pore sizes.[23,24] Both MIL-53 and MIL-68 have been synthesized and studied for potential applications by several research groups.[25,26] Aluminum-based MOFs are especially interesting due to their high thermal stability (>500 °C) and relatively low synthesis costs.[27] While many reports exist on the synthesis of MIL-53(Al) with Al^{3+} as the metal center,[18,28–30] the synthesis of MIL-68(Al) is more challenging.[31] Often, the synthesis protocols for MIL-68(Al) result in a mixture of MIL-53(Al) and MIL-68(Al).[32] Consequently, the decisive parameters leading to the formation of either MIL-53(Al) or MIL-68(Al) under different synthesis conditions are not understood.[31] Recently, Wu *et al.* reported that increasing the metal to linker ratio during MIL-68(In) synthesis from NH_2–, Br–, and NO_3–H_2BDC induced the formation of MIL-68(In) rather than MIL-53(In).[33]

To investigate this framework isomerism, we chose a modulated synthesis approach. The addition of monocarboxylic acid modulators during MOF synthesis has been shown in numerous studies to influence and control the particle size and shape,[34,35] and sometimes to increase the reproducibility, crystallinity and surface area of the targeted MOF structures.[36–38] The modulation capabilities of formic acid are heavily dependent on the chemical environment and system under investigation.[38,39] Generally, they are believed to influence MOF synthesis by either lowering the local pH and decreasing the linker deprotonation rate, or by competitively coordinating with the metal center in place of the linker and slowing down MOF nucleation.[34,38–40] However, the formation of such competitive coordination species in solution and effect of carboxylic acids on the development of intermediate species that combine and reassemble to form the final MOF products have, to the best of our knowledge, not yet been directly studied with *in situ* synthesis monitoring methods.

2. Experimental section

2.1 MIL-53/MIL-68(Al) synthesis

Terephthalic acid (≥98%, Merck Chemicals GmbH), $Al(NO_3)_3$·$9H_2O$ (≥98%, Carl Roth GmbH + Co), DMF (≥99.5%, Carl Roth GmbH + Co), Na_2BDC (≥99%, Alfa Aesar), $NaHC(O)O$ (≥98%, Alfa Aesar), HNO_3 (≥65%, Carl Roth GmbH + Co) and formic acid (≥99%, Analor normapur) were purchased from commercial suppliers and used without further purification.

MIL-53(Al) and MIL-68(Al) were synthesized in a 1.5 liter Büchi Versoclave Type 3E reactor described in previous studies.[28] 0.165 M of terephthalic acid (H_2BDC) and 0.33 M of $Al(NO_3)_3$·$9H_2O$ were first stirred for at least 30 min in a 0.5 l DMF-based solution, which for some synthesis contained 2.5 mol l^{-1} formic acid. The addition of 2.5 M formic acid to 0.165 M terephthalic acid dissolved in DMF caused the solution to become slightly turbid. The mixture was then decanted into the reactor and heated over 4 h to the desired synthesis temperature (50–100 °C) under constant stirring conditions (240 rpm). After synthesis, the reactor was cooled to room temperature. The product as washed in ethanol with three centrifugation and redispersion cycles prior to particle characterization. Part of the product was calcined at 400 °C for 18 h to remove unreacted organic linker and solvent molecules from the pores.

2.2 Product characterization

Raman spectra of the synthesis solution were acquired every 3 min with a Wethead™ liquid-phase probe and Kaiser Optics RAMANRXN1 analyzer system. Measurements were taken with a 0.5 W 785 nm laser between 175–3425 cm^{-1} with a 2 min exposure time and resolution of 4 cm^{-1}. The integrated areas of the (νCC + δCH) MIL-53(Al) band at 1148 cm^{-1} and $\delta(COO^-)$ PNBU band at 780 cm^{-1} (ref. 28, 41 and 42) were converted to their equivalent areas at 25 °C, as described elsewhere.[28] Fourier-transform infrared (FTIR) spectra were acquired during synthesis every 5 min with an art photonics diamond attenuated total reflection tip connected to a Bruker Instruments Matrix MF system. Measurements with a resolution of 4 cm^{-1} were taken between 700 and 1900 cm^{-1} from 32 accumulated scans.

A Gemini SEM 500 scanning electron microscope (SEM) was operated at 1 kV to obtain images of the MOF particles. A milky white MOF suspension in ethanol was dropped onto a silicon wafer for imaging. The average length and standard deviation along the longest length direction of at least 200 particles was measured with the ImageJ software. N_2 sorption isotherms at 77 K were measured with a Micromeritics ASAP 2010 sorption analyzer. Samples were outgassed for 20 h at 250 °C prior to the measurements. The procedure of Rouquerol *et al.* was used to select the relative pressure range for the Brunauer–Emmett–Teller (BET) area calculations.[43] For X-ray diffraction (XRD) measurements, a PANalytical Empyrean diffractometer with a CuKα X-ray source operated at 40 kV und 40 mA was employed. An angular 2θ range from 3 to 50°, a scan step time of 47.6 s and step size of 0.00179° was used. For thermogravimetric analysis (TGA) measurements in air, a TA Instruments TGA 2950 employing a heating ramp of 5 K min^{-1} was used. *Ex situ* Fourier-transform infrared (FTIR) spectra were taken with a JASCO FT/IR-4100 spectrometer and Pike Technologies Glad-iATR attenuated total reflection unit. 16 scans with a resolution of 4 cm^{-1} were accumulated.

3. Results and discussion

3.1 Particle properties

MIL-53(Al) and MIL-68(Al) were synthesized from a H_2BDC and $Al(NO_3)_3$·$9H_2O$ solution in DMF with and without 2.5 M formic acid modulation heated to 100 °C and 80 °C for 17 h and to 60 °C, 55 °C and 50 °C for 90 h. The heating time was extended at the

lower synthesis temperatures to allow MOF formation to reach completion and to enable extraction of kinetic data. Unmodulated synthesis at temperatures between 50 and 100 °C resulted in the formation of MIL-53(DMF) with DMF in the pores, as indicated by the characteristic XRD reflexes at $2\theta = 9.1°$, $10.0°$ and $18.3°$ in Fig. 1a.

In contrast, a mixture of MIL-53(DMF) and MIL-68 ($2\theta = 4.8°$, $8.4°$ and $9.7°$) formed from synthesis with 2.5 M formic acid modulation. 2.5 M was identified as the optimal formic acid concentration to induce MIL-68(Al) formation (Fig. S4†). A large excess of formic acid with respect to H_2BDC (0.165 M) and $Al(NO_3)_3 \cdot 9H_2O$ (0.33 M) was required for MIL-68(Al) formation to occur. When the synthesis temperature was lowered from 100 °C to 55 °C upon modulation with 2.5 M formic acid, the fraction of MIL-68 in the product increased continuously (Fig. 1a). Almost phase pure MIL-68(Al) was formed at 55 °C. Views of the crystal structures of MIL-53(Al) and MIL-68(Al) and their Al octahedra chains are compared in Fig. 1b.

Unmodulated synthesis in DMF at $50 \le T \le 100$ °C resulted in the growth of nanoplatelets < 100 nm in length (Fig. 2a–c). Furthermore, the N_2 isotherms of the product of unmodulated syntheses had a pronounced gas uptake at $p/p_0 > 0.9$ from N_2 condensation in the interstitial voids between the nanoparticles (Fig. S5†). Modulation with 2.5 M formic acid results in a dramatically increased particle size. Elongated oval-shaped particles around 2 μm in length were formed upon formic acid modulation at $55 \le T \le 100$ °C (Fig. 2d–f). Due to the larger particle size, the N_2 sorption isotherms of the samples synthesized with formic acid modulation had no additional uptake at $p/p_0 > 0.9$ (Fig. S5†). The BET areas of the samples determined *via* N_2 sorption were all between 1050 and 1470 m^2 g^{-1} (Table S1†).

The product of 2.5 M formic acid modulated synthesis at 55 °C was isolated after various synthesis times and subjected to heating at an elevated temperature (120 °C) to test if one of the two MIL isomers was the intermediate product and the other the thermodynamically stable product. The ($\nu CC + \delta CH$) Raman MOF band at 1148 cm^{-1} began to form after 40 h of heating, reached its maximum intensity after 65 h, and then remained constant for the remainder of synthesis (Fig. 3a). MIL-53(Al) and MIL-68(Al) were confirmed to both share identical Raman and FTIR bands (Fig. S2 and S3†). Fig. 3b and c shows the typical evolution of the ($\nu CC + \delta CH$) band at 1148 cm^{-1} and the PNBU δCOO^- at 785 cm^{-1}, respectively, at 80 °C monitored by Raman spectroscopy.

Poorly crystalline MIL-68(Al) was isolated at the onset of MOF formation after 42 h of heating, as visible in the corresponding XRD pattern (Fig. 3d). The XRD patterns indicate an increase in MIL-68(Al) crystal coherence length, coinciding with an increase in particle size (Fig. 4), between 42 and 90 h. Between 90 and 164 h, the MIL-68 XRD reflex intensity decreased while a shoulder at $2\theta = 9.1$ from MIL-53(DMF) containing DMF molecules in the pores appeared. This indicates that, between 90 and 164 h, part of the MIL-68 product was converted into MIL-53. Similar conclusions were drawn from a temperature study, where the reaction solution after 164 h synthesis at 55 °C, containing mostly MIL-68(Al) and a small amount of MIL-53(DMF), was heated to 120 °C for an additional 48 h. After heating the solution at 120 °C, the MIL-68 reflexes shrank and the MIL-53 reflexes increased in intensity as MIL-68 was further converted into the MIL-53 phase (Fig. 3d).

The washed (three times centrifuged in ethanol) product at the onset of MIL-68(Al) formation after 42 h and also after 90 h contained only water in the pores, as shown by the
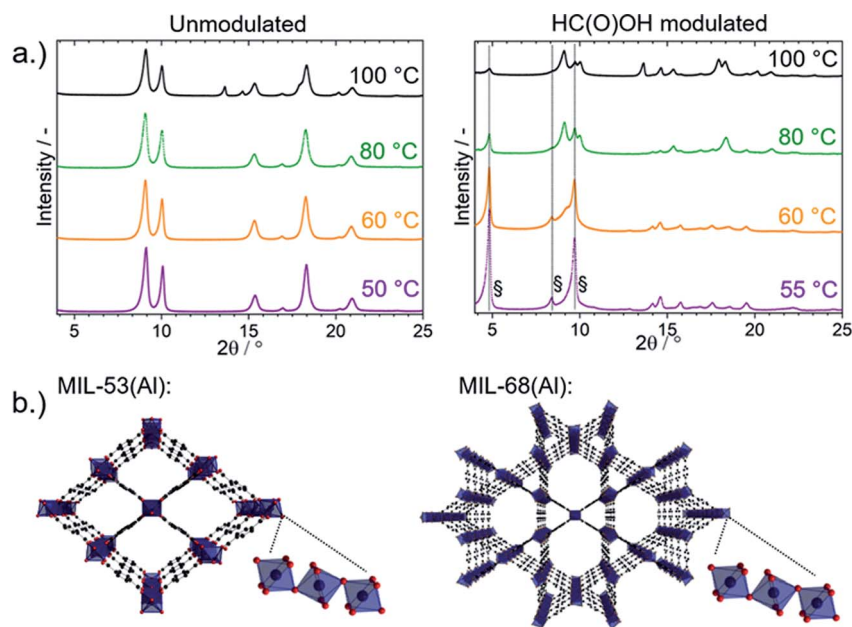

Fig. 1 (a) XRD patterns of the products from synthesis in DMF at various temperatures both without and with 2.5 M formic acid modulation. § = MIL-68(Al). (b) Diagrams of the MIL-53(Al) and MIL-68(Al) crystal structures.
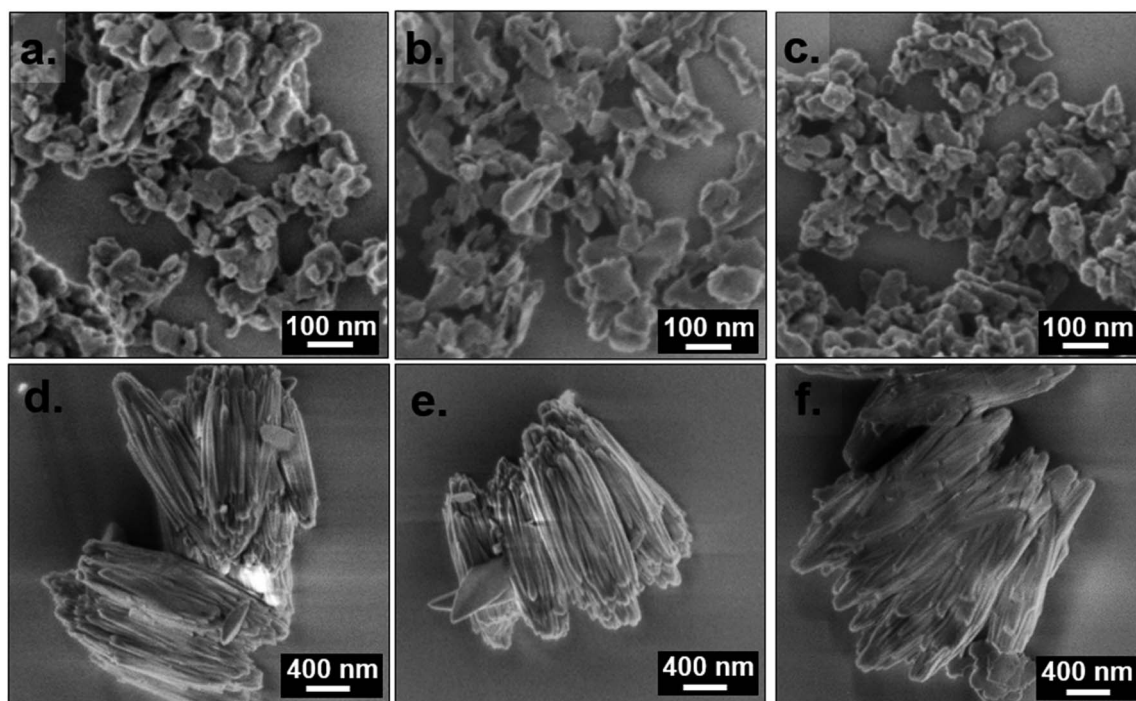
Fig. 2 SEM images of MOF particles synthesized in DMF without formic acid modulation at (a) 100 °C (17 h), (b) 80 °C (17 h) and (c) 60 °C (90 h), and with 2.5 M formic acid modulation at (d) 100 °C (17 h), (e) 80 °C (17 h), (f) 55 °C (90 h).

corresponding IR bands at 989 cm^{-1} from δ(OH) of the bridging OH groups in the MOF,[42,44] the absence of IR bands from DMF or H$_2$BDC in the pores at 1670 or 1699 cm^{-1}, respectively (Fig. 3e) and the presence of a weight loss below 100 °C in the TGA profiles (Fig. S6a†). The intensity of the δ(OH) IR band is known to be remarkably reduce in the presence of DMF, as reported by Kriesten *et al.*[32] The unwashed product of the 42 h synthesis, however, contained DMF in the pores. This is indicated by the FTIR band assigned to the carbonyl group of DMF at 1670 cm^{-1} and the TGA weight loss centered at 140 °C in Fig. S7.† The pores of MIL-68(Al), thus, initially form around DMF molecules rather than around H$_2$BDC molecules, as has been previously reported to be the case for MIL-53(Al).[18,28] While the flexible pores of MIL-53(Al) strongly adsorb to guest molecules and prevent their removal during the washing step,[18] the rigid MIL-68(Al) pores do not adsorb guest molecules, which are evidently removed during centrifugation in ethanol. The appearance of a band in the FTIR spectra at 1660 cm^{-1} assigned to the carbonyl group of DMF and a weight loss centered at 140 °C in the TGA profiles (Fig. S6†) in the mixed MIL-53/MIL-68(Al) product isolated after heating at 120 °C indicates that the newly formed MIL-53(Al) phase contained DMF in the pores, even after washing.

The MIL-68(Al) product isolated after 42 h heating at 55 °C consisted exclusively of egg-shaped particles with a length of ≤ 0.5 μm. These grew into 2 μm long ribbed particles after 90 h (Fig. 4). The product of 164 h synthesis, which was mostly MIL-68(Al), was likewise composed only of 2 μm long ribbed particles. After heating the synthesis mixture for 48 h at 120 °C, the mixed MIL-53/MIL-68(Al) product contained smaller particles with a smooth texture in

addition to the afore-mentioned 2 μm long ribbed particles. Also, it was possible to observe particles with smooth surfaces branching off the ribbed particles (Fig. 4, black frame). The fact that the partial conversion of MIL-68(Al) into MIL-53(Al) is accompanied by the formation of new particles exhibiting a different morphology suggests that the conversion occurred through a particle dissolution-recrystallization process rather than a solid-phase rearrangement.

Thus, it has to be assumed that MIL-68(Al) is the kinetically favored intermediate product and MIL-53(Al) the thermodynamically stable product of formic acid modulated synthesis in DMF. The additional steric strain acting on μ-OH groups confined in the small triangular pores of the MIL-68(Al) structure (depicted in Fig. S8†) results in a lower thermal stability of this phase compared to MIL-53(Al). The relationship between MIL-68(Al) and MIL-53(Al) appears analogous to that previously determined by Gascon *et al.* for the kinetically favored intermediate NH$_2$-MIL-101(Al) and thermodynamically stable NH$_2$-MIL-53(Al) phases.[13–15] An intermediate NH$_2$-MIL-235 phase formed prior to NH$_2$-MIL-53(Al) was also reported to convert to NH$_2$-MIL-53(Al) through a dissolution-recrystallization process.[13]

3.2 *In situ* synthesis monitoring

To shed light on the mechanism by which formic acid induces the formation of MIL-68(Al) micro-particles rather than MIL-53(Al) nanoplatelets, the synthesis solution was studied with *in situ* Raman and FTIR spectroscopy. The framework isomers MIL-53(Al) and MIL-68(Al) were confirmed to share identical FTIR and Raman bands (Fig. S2 and S3†).
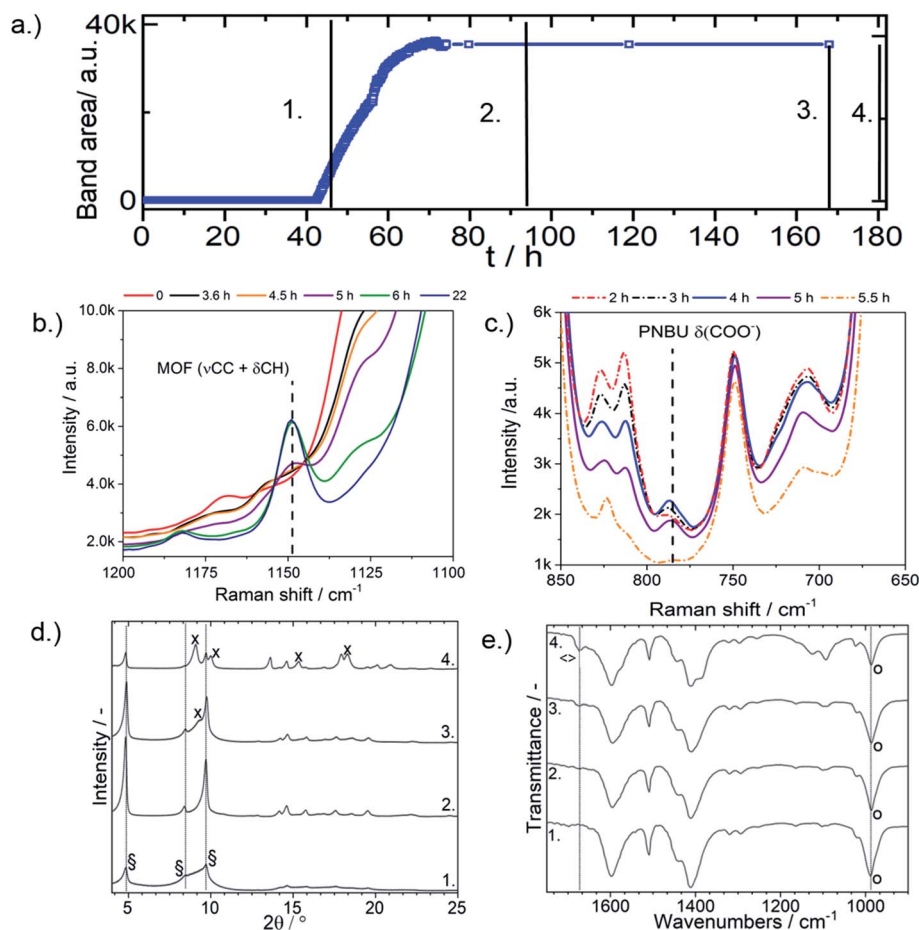
Fig. 3 (a) Area of the *in situ* Raman (νCC + δCH) MOF band during formic acid modulated synthesis at 55 °C. Black lines indicate the studied synthesis times. (b) and (c) Raman spectra of the reaction mixture at 80 °C. (d) XRD patterns, and (e) FTIR spectra of samples of formic acid modulated synthesis at 55 °C after (1) 42 h, (2) 90 h, (3) 164 h heating and (4) after an additional 48 h heating at 120 °C. § = MIL-68. x = MIL-53(DMF). $\langle\rangle$ = MIL(DMF). o = MIL(H$_2$O).

The first step of MIL-53(Al) synthesis was identified in a previous study as the coordination of the metal center with the H$_2$BDC linker to form intermediate Al-HBDC prenucleation building unit (PNBU) complexes dissolved in solution, followed by the assembly and rearrangement of the PNBUs into MIL-53(Al).[28] The temporal evolution of the characteristic Raman bands of δ(COO$^-$) of the intermediate PNBU species and (νCC + δCH) of the MOF product for both unmodulated and formic acid modulated synthesis is compared in Fig. 5. Formic acid modulation caused both PNBU formation and crystallization to begin significantly later and occur at a slower rate than for unmodulated synthesis at the corresponding synthesis temperatures. Modulation with monocarboxylic acids was likewise shown in studies of Zr MOF and MIL-101(Cr) synthesis to decrease the MOF growth rate and promote the formation of larger particles.[36–38]

As shown in the Raman profiles, the accumulation of PNBUs prior to the precipitation of the MOF was significantly reduced upon formic acid modulation (Fig. 5). The kinetic growth rate constants and activation energies of both PNBU and MOF formation were calculated using the Avrami and Arrhenius

equations (Fig. S9†) as described in a previous study.[28] The calculated PNBU activation energy of formation increased from 66 ± 3 kJ mol^{-1} to 77 ± 3 kJ mol^{-1} upon modulation with formic acid (Table 1). In contrast, the activation energy of the MOF formation, which was determined to around 90 kJ mol^{-1}, remained unaffected by formic acid modulation. The increase in PNBU formation energy and constant MOF formation energy upon formic acid modulation indicates that formic acid affects the synthesis by influencing the formation of intermediate species predominantly in the early stages of MOF formation.

The increase of the activation energy of PNBU formation from 66 to 77 kJ mol^{-1} upon formic acid modulation evidently caused a lower concentration of PNBUs to be present in solution when the 90 kJ mol^{-1} activation energy of MOF formation had been reached. This reduced the nucleation rate and favoured the growth of larger particles compared to the unmodulated synthesis.

Unmodulated synthesis at 50 °C, with a kinetic formation rate constant of 0.10, resulted in formation of phase pure MIL-53(Al) product. Formic acid modulated synthesis at 80 °C had a significantly higher kinetic MOF formation rate constant of
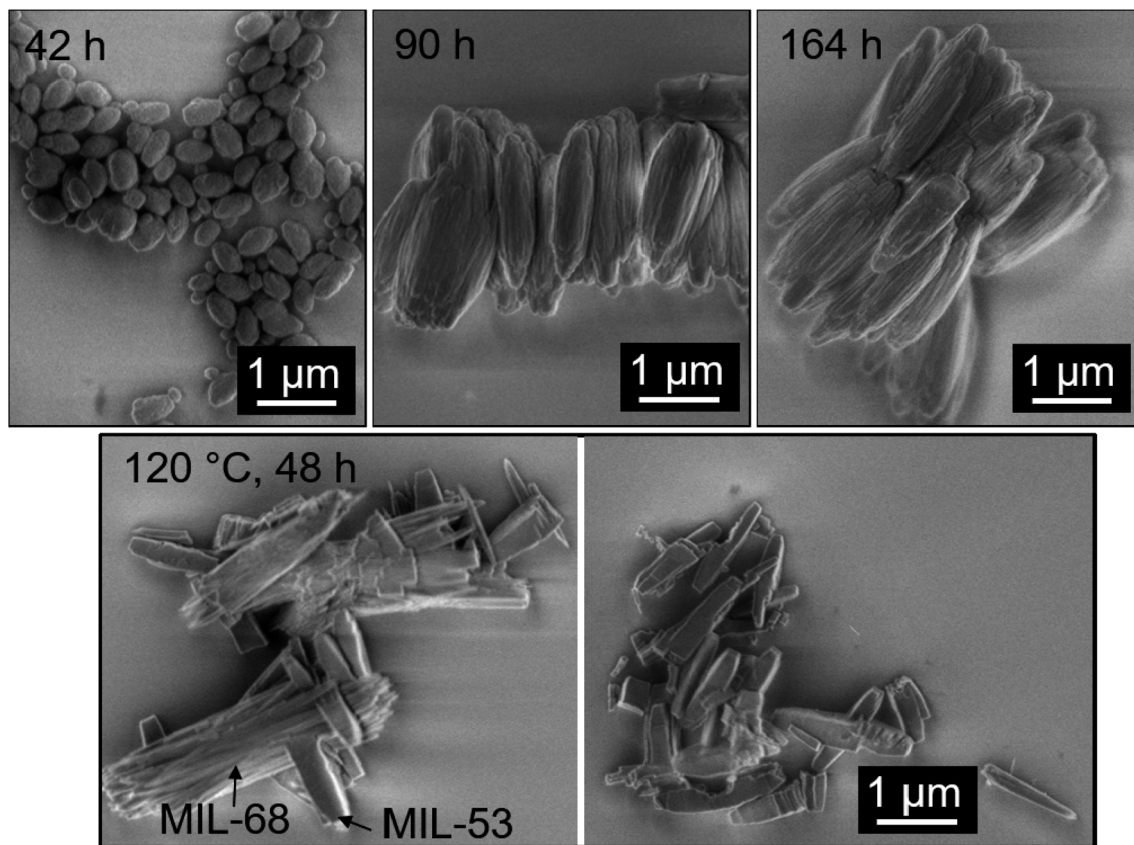
Fig. 4 SEM images of the MOF product after 42, 90, and 164 h synthesis at 55 °C and after an additional 48 h heating at 120 °C.
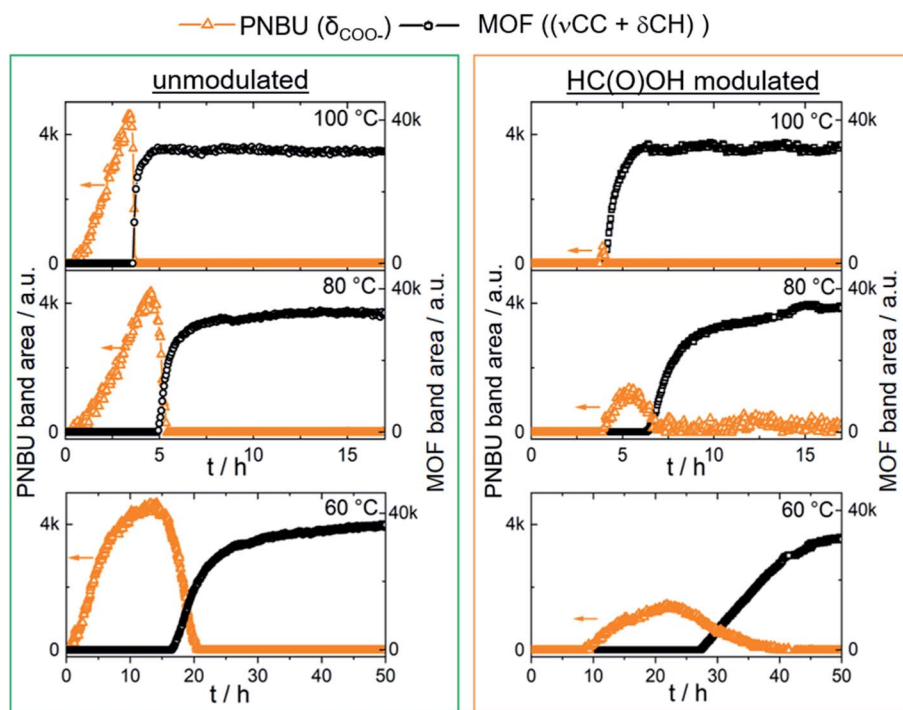

Fig. 5 Evolution of the characteristic *in situ* Raman PNBU and MOF band areas during MOF synthesis in DMF with and without formic acid modulation.

Table 1 Induction time before the onset of PNBU formation, maximum *in situ* area of the characteristic Raman PNBU band, and calculated PNBU and MOF growth rate constants and activation energies of formation and particle size for synthesis in DMF with and without formic acid modulation

	$T/°C$	t_o PNBU/h	Max band area/a.u.	E_a PNBU/kJ mol^{-1}	k_{MOF}/h^{-1}	$m_{MOF}/—$	E_a MOF/kJ mol^{-1}
Ref.	50	1.8	3800	66 ± 3	0.10	1.3	90 ± 8
	60	0.8	3900		0.22	1.4	
	80	0.4	4200		1.5	1.0	
HC(O)OH mod.	60	6.0	1400	77 ± 3	0.10	1.3	91 ± 5
	80	4.0	1000		0.55	1.3	
	100	3.8	800		3.69	1.0	

0.55, but nevertheless resulted in the growth of a MIL-68/MIL-53(Al) phase mixture. Therefore, the formation of MIL-68(Al) rather than MIL-53(Al) at low synthesis temperatures upon formic acid modulation cannot be ascribed solely to the reduced MOF formation rate. Instead, specific interactions between formic acid and either the metal center or the H$_2$BDC linker are believed to change the synthesis solution properties to trigger MIL-68(Al) formation.

MIL-53(Al) was synthesized in the presence of 33 mM of nitric acid to introduce the same proton concentration in solution as during modulation with 2.5 M of formic acid in order to test if the modulation capabilities of formic acid are caused by a decrease in local pH. To minimize the measurement time of the *in situ* Raman device, the synthesis was carried out at 80 °C (17 h) rather than 55 °C (90 h). The amount of water added to the synthesis mixture through the addition of 33 mM of 65 vol% nitric acid (0.37 ml water to 500 ml reaction solution) was negligible in comparison to the 27 ml water in solution originating from the Al(NO$_3$)$_3$·9H$_2$O salt. MIL synthesis with 33 mM nitric acid resulted in the formation of MIL-53(DMF) nanoplatelets and no change in the PNBU or MIL-53(Al) growth profile as compared to the reference synthesis without acid addition (Fig. S10†). This indicates that the formic acid modulation mechanism is not driven by a drop in solution pH.

Next, *in situ* Raman spectroscopy was employed to test if formic acid competitively coordinates to the Al^{3+} center or if it rather interacts with the H$_2$BDC linker. Both interactions are possible, but only the former was discussed by other authors.[34,38–40] However, it was not possible to differentiate between terephthalate and formate coordinated to Al^{3+} with Raman spectroscopy. Solutions of Al(NO$_3$)$_3$·9H$_2$O mixed with either Na$_2$BDC or NaHC(O)O in DMF both contained an identical Raman band at 780 cm^{-1} from δ(COO$^-$) [Al-HBDC] or δ(COO$^-$) [Al-HC(O)O], respectively (Fig. 6a).[28]

To compare the relative coordination rates of both terephthalate and formate with Al^{3+}, Raman spectra were collected during a blank experiment where 0.33 M Al(NO$_3$)$_3$·9H$_2$O was heated to 80 °C in DMF in the presence of either 0.165 M of H$_2$BDC or 0.165 M or 2.5 M of formic acid. In all three cases, a Raman band at 780 cm^{-1} from δ(COO$^-$) of the complexes [Al-HBDC] or [Al-HC(O)O] formed after a certain induction period and grew linearly in intensity with time (Fig. 6b). In the H$_2$BDC-containing solution, the δ(COO$^-$) Raman band appeared a few hours earlier than and increased at about 6.6 times the rate of

the δ(COO$^-$) Raman band observed in the solution with 0.165 M formic acid. This indicates that terephthalate coordinates much more rapidly than formate with Al^{3+}, even when the formic acid concentration (2.5 M) was much higher. This observation can be explained by the higher tendency of terephthalic acid to deprotonate compared to formic acid. The pK_{a1} of H$_2$BDC (3.5) is lower than that of formic acid (3.8).[45] Although the blank heating experiments were carried out in the aprotic solvent DMF, it must be noted that the solutions contained 3 M of water from the hydrated aluminum salt. Thus, the water molecules in solution should be able to accept protons from the carboxylic acid groups.

Terephthalate and formate coordinated to Al^{3+} can be differentiated from one another with FTIR spectroscopy. When formate is coordinated to Al^{3+}, the FTIR δ(COO$^-$) vibration mode undergoes band splitting due to crystal field effects.[46] In consequence, the DMF solution of Al(NO$_3$)$_3$·9H$_2$O and NaHC(O)O contained two FTIR bands at 773 and 790 cm^{-1} from δ(COO$^-$) of the complex [Al-HC(O)O] (Fig. 7a). The presence of two such bands from a COO$^-$ vibrational mode of formate coordinated to aluminum were previously confirmed in both inelastic tunnelling spectroscopy and FTIR studies.[46] In contrast, Al(NO$_3$)$_3$·9H$_2$O mixed with Na$_2$BDC in DMF exhibits only one FTIR band at 780 cm^{-1} from δ(COO$^-$) of the PNBU [Al-HBDC] (Fig. 7a).[28] The δ(COO$^-$) PNBU [Al-HBDC] band presumably does not undergo splitting because the benzene ring stabilizes HBDC$^-$, causing terephthalic acid to form a weaker coordination complex with Al^{3+} compared to formic acid.

During formic acid modulated MOF synthesis at 80 °C, an intermediate FTIR band at 780 cm^{-1} from the PNBU [Al-HBDC], but no bands at 773 or 790 cm^{-1} from [Al-HC(O)O] are formed (Fig. 7b). The much faster coordination rate of H$_2$BDC than formic acid to Al^{3+} coupled with the absence of characteristic *in situ* FTIR bands from a [Al-HC(O)O] coordination complex during formic acid modulation raises doubts that MIL-68(Al) formation is caused by competitive coordination between the modulator and the linker with the Al^{3+} metal center.

Formic acid was instead observed in the Raman spectra to form double hydrogen-bonds with the carboxylic acid group of the linker H$_2$BDC. Aromatic carboxylic acids are known to form strong double H-bonds, strengthened by π-conjugation, with one another in solution.[47] The estimated double H-bonding energy of the benzoic acid dimer, which resembles H$_2$BDC with only one carboxylic acid group, is −13.9 kJ mol^{-1} whereas
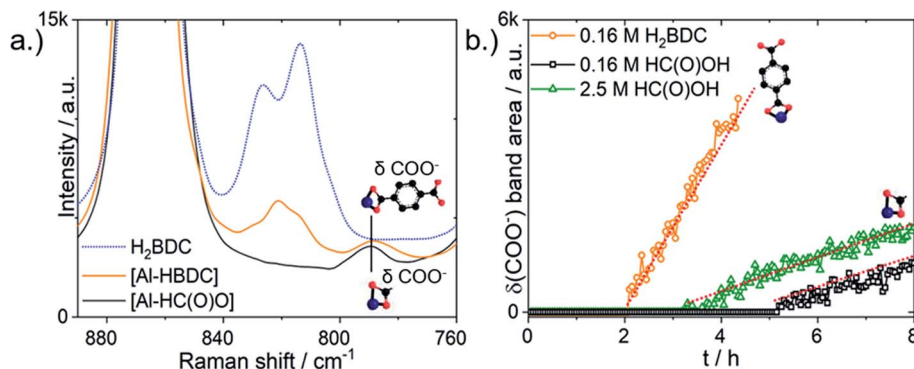
Fig. 6 (a) Raman spectra of H_2BDC, [Al–HBDC] and [Al–HC(O)O] in DMF. (b) Evolution of the $\delta(COO^-)$ Raman band area during heating in DMF at 80 °C of $Al(NO_3)_3 \cdot 9H_2O$ with either 0.165 M H_2BDC or 0.165 or 2.5 M formic acid.

that of the formic acid dimer is −12.9 kJ mol^{-1}.[48] Adding 2.5 M of formic acid to 0.33 M of H_2BDC in DMF caused the intensities of the H_2BDC Raman ring breathing doublet bands at 814 and 826 cm^{-1} and the $\nu(CC)$ band at 1612 cm^{-1} to decrease (Fig. 8a). New red-shifted bands formed in their place at 833 and 1633 cm^{-1}. Similar Raman band positions were previously detected for H-bonded H_2BDC in water. Therefore, the red shift of the Raman H_2BDC bands upon addition of formic acid is attributed to the formation of H-bonding complexes between H_2BDC and formic acid. Upon addition of 2.5 M of formic acid to 0.33 M of H_2BDC in DMF, the initially clear solution turned turbid. No new resonances appeared in the ^{13}C-NMR spectra, allowing chemical reactions between H_2BDC and HC(O)OH to form a new species to be ruled out (Fig. S11†).

H-bonding between H_2BDC and formic acid was directly observed *in situ* during formic acid modulated synthesis from 0.66 M of $Al(NO_3)_3 \cdot 9H_2O$ and 0.33 M of H_2BDC. Intense Raman bands at both 1614 and 832 cm^{-1} from H_2BDC H-bonded with formic acid were present in the precursor solution prior to heating (Fig. 8b, step 1). After 3.5 h of heating, these bands decreased in intensity and shifted to lower wavenumbers, *viz.* closer to the position of free H_2BDC (Fig. 8b, step 2). PNBU formation did not begin until after 5 h, at which point the Raman H_2BDC ring breathing bands had almost completely

shifted to the position of non H-bonded H_2BDC vibrations (Fig. 8b, step 3).

Fig. 9 depicts the two possible pathways of formic acid modulation – hydrogen bonding with the H_2BDC linker and competitive coordination with the Al^{3+} metal center. As indicated in Fig. 6a, both formate and terephthalate coordinated to Al^{3+} exhibit an identical $\delta(COO^-)$ Raman band at 780 cm^{-1}. Therefore, if synthesis modulation occurs due to competitive coordination, the maximum intensity of the intermediate $\delta(COO^-)$ Raman band during MIL-68/MIL-53(Al) formation should remain unaffected. In contrast, the H-bonding carboxylic groups do not show a $\delta(COO^-)$ Raman band at 780 cm^{-1}. H-bonds between H_2BDC and formic acid increase the activation energy and slow the rate of PNBU formation, but do not affect the self-assembly rate of PNBUs into the MOF framework. This causes reduced PNBU accumulation prior to MOF precipitation and should result in the formation of a less pronounced intermediate $\delta(COO^-)$ Raman band prior to the onset of MOF growth. Indeed, the $\delta(COO^-)$ Raman band intensity at 780 cm^{-1} is reduced by about 66% during the formic acid modulated synthesis (Fig. 5). The reduced intensity of the intermediate $\delta(COO^-)$ Raman band observed upon formic acid modulation provides further evidence for the suggested modulation mechanism involving hydrogen bonding of formic acid with the
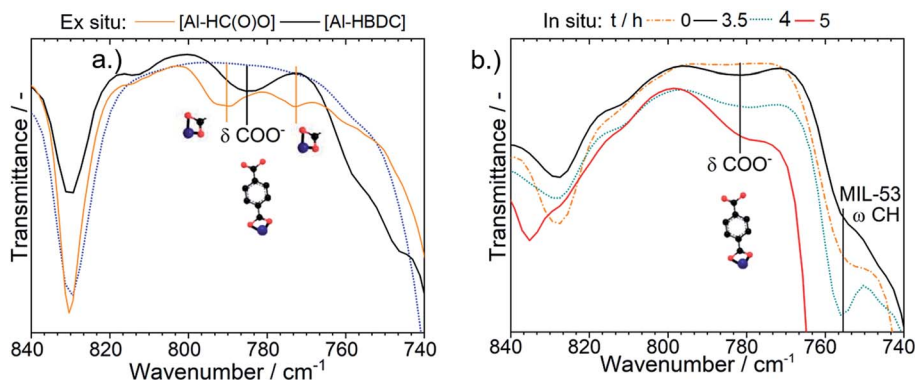

Fig. 7 (a) FTIR spectra of H_2BDC (blue dotted line), [Al–HBDC] and [Al–HC(O)O] in DMF. (b) FTIR spectra collected at selected time points during formic acid modulated synthesis in DMF at 80 °C.
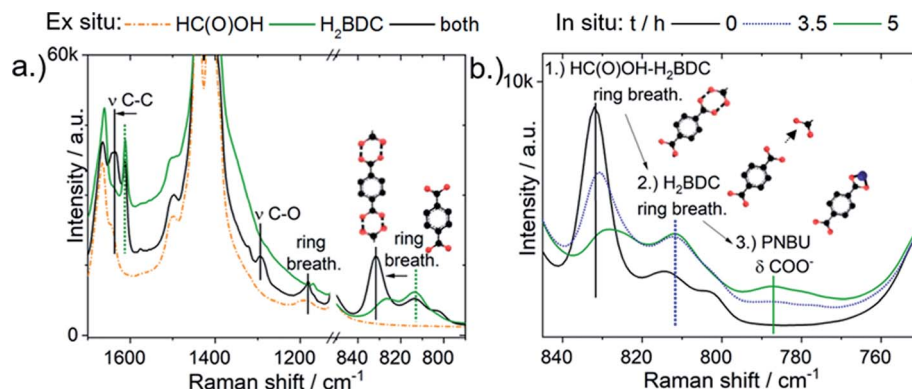
Fig. 8 (a) Raman spectra of formic acid, H_2BDC, and both H_2BDC and formic acid in DMF with annotated H_2BDC vibrational modes. (b) Raman spectra collected at selected times during formic acid modulated synthesis at 80 °C.

H_2BDC linker rather than a competitive coordination mechanism with the Al center.

3.3 Rationale for MIL-68(Al) formation

In previous studies, MIL-53(Al) was shown to initially form with unreacted H_2BDC in the pores, despite the concentration of the DMF solvent (13 M) being much higher than that of H_2BDC (0.165 M).[28] H_2BDC in the pores was replaced with DMF solvent molecules upon linker depletion in a later stage of the synthesis. Interactions between H_2BDC guest molecules and the MIL-53(Al) framework are apparent as the pore dimensions increase from 7.3×7.7 Å^2 to 8.5×8.5 Å^2 upon removal of H_2BDC from the pores.[18] As previously alluded by Loiseau *et al.*,[18] it is likely that a portion of the unreacted linker serves as a template in the initial formation of the rhombic MIL-53(Al) pores. Both neutral and charged molecules are known to serve as templating agents during the formation of zeolites, a related family of microporous crystals to MOFs.[49] In contrast to MIL-53(Al), MIL-68(Al) was observed in this study to initially form with DMF rather than H_2BDC in the pores (Fig. S7†). The 6–6.4 Å

triangular channels of MIL-68(Al) are too small, while the rigid 16–17 Å hexagonal MIL-68(Al) pores are too large to form around H_2BDC as molecular template.

During unmodulated synthesis in DMF, the high availability of H_2BDC in solution promotes the formation of MIL-53(Al), even at low temperatures and short synthesis times, rather than MIL-68(Al) due to this templating function. By forming H-bonded dimers or trimers of formic acid with H_2BDC in solution, the modulator formic acid (2.5 M) could prevent free H_2BDC (0.165 M) from serving as a template for the rhombic pores of MIL-53(Al). This triggers the formation of the kinetically favored product MIL-68(Al) containing DMF rather than H_2BDC in the triangular pores at low synthesis temperatures as depicted in the schematic of Fig. 10. In the field of zeolite formation, the availability of species in solution acting as templating molecules have often been reported to play an important role in determining the final crystal structure.[49,50]

Along related lines, Volkringer *et al.* observed the formation of MIL-68(Ga) with DMF rather than H_2BDC in the triangular pore channels. They proposed that DMF molecules, which had
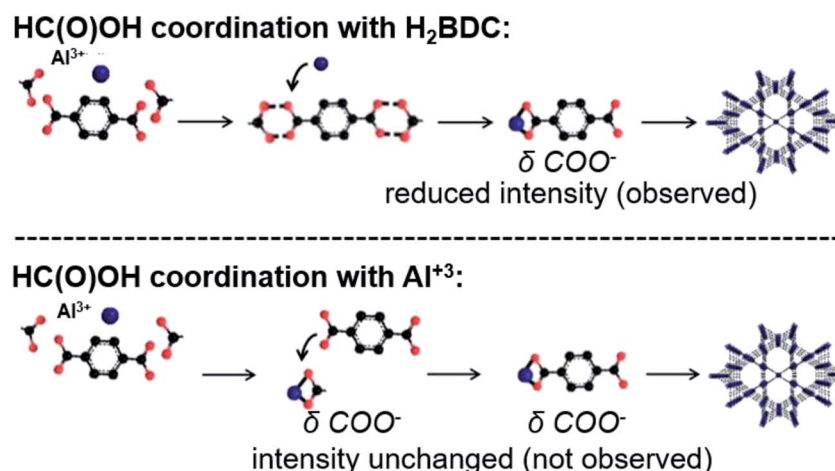

Fig. 9 Two possible formic acid modulation mechanisms and their theoretical effect on the intermediate $\delta(COO^-)$ Raman band at 780 cm^{-1}.
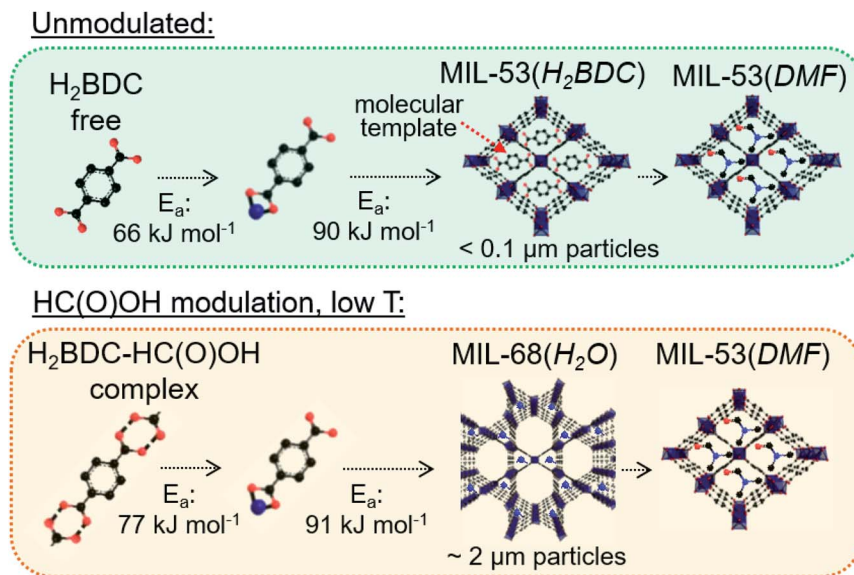
Fig. 10 Proposed relationship between formic acid modulation in DMF and MIL-68(Al) formation.

strong H-bonding interactions with the MOF hydroxyl groups, play a templating role in the formation of MIL-68(Ga) triangular pore channels.[21] The connection between synthesis conditions causing a H_2BDC deficiency in solution and MIL-68 formation reported here are also consistent with a study by Wu and colleagues. They reported that an excess of metal precursor with respect to the organic linker in the synthesis mixture caused the formation of $-NH_2$, $-Br$, and $-NO_2$ functionalized MIL-68(In) rather than MIL-53(In).[33]

4.   Conclusions

Formic acid modulation induces the formation of MIL-68(Al) at low synthesis temperatures in DMF. MIL-68(Al) is identified as the kinetically favored intermediate product of formic acid modulated synthesis, which converts into the thermodynamically stable MIL-53(Al) product after prolonged synthesis times and elevated temperatures.

Formic acid modulation slowed both prenucleation building unit (PNBU) formation and MOF crystallization and increased the PNBU formation activation energy from 66 ± 3 kJ mol^{-1} to 77 ± 3 kJ mol^{-1}. Our data indicate that formic acid's modulation capabilities stem from the formation of hydrogen bonds between the carboxylic acid groups of the modulator and the linker H_2BDC rather than the commonly assumed mechanism involving competitive coordination of formic acid with the metal center Al^{3+}. H_2BDC is proposed to serve as a molecular template for the rhombic MIL-53(Al) structure, which initially forms around unreacted H_2BDC molecules. In contrast to MIL-53(Al), MIL-68(Al) initially forms with DMF in the pores. By forming coordination complexes with H_2BDC in solution, formic acid could prevent free H_2BDC from serving as a molecular template for the MIL-53(Al) structure, allowing the formation of

the kinetically favored (intermediate) MIL-68(Al) product at low temperatures and short synthesis times.

The present study contributed to an improved understanding of the controlled synthesis of the two Al MOF isomers MIL-53(Al) and MIL-68(Al). Furthermore, the methodology presented herein using *in situ* Raman and FTIR spectroscopy can generally be applied to gain a better mechanistic understanding of carboxylic acid modulated synthesis for a variety of MOF materials.

Abbreviations

a.u.	Arbitrary units
BDC	Terephthalate
BET	Brunauer, Emmett and Teller
E_a	Activation energy
EDXRD	Energy dispersive X-ray diffraction
DMF	*N,N*-Dimethylformamide
FTIR	Fourier-transform-infrared
H_2BDC	Terephthalic acid
MIL	French. Matériaux de l'Institut Lavoisier
MOF	Metal–organic framework
PNBU	Prenucleation building unit
SAXS	Small angle X-ray scattering
SBU	Secondary building units
SEM	Scanning electron microscopy
TGA	Thermogravimetric analysis
XRD	X-ray diffraction

Author contributions

All authors have given approval to the final version of the manuscript.

Conflicts of interest

No potential conflict of interest was reported by the authors.

Acknowledgements

References

1 H. Furukawa, K. E. Cordova, M. O'Keeffe and O. M. Yaghi, The Chemistry and Applications of Metal–Organic Frameworks, *Science*, 2013, **341**, 1230444, DOI: 10.1126/science.1230444.

2 M. Hartmann, U. Böhme, M. Hovestadt and C. Paula, Adsorptive Separation of Olefin/Paraffin Mixtures with ZIF-4, *Langmuir*, 2015, **31**, 12382–12389, DOI: 10.1021/acs.langmuir.5b02907.

3 M. Hovestadt, S. Friebe, L. Helmich, M. Lange, J. Möllmer, R. Gläser, A. Mundstock and M. Hartmann, Continuous Separation of Light Olefin/Paraffin Mixtures on ZIF-4 by Pressure Swing Adsorption and Membrane Permeation, *Molecules*, 2018, **23**, 889–902, DOI: 10.3390/molecules23040889.

4 D. Himsl, D. Wallacher and M. Hartmann, Improving the Hydrogen-Adsorption Properties of a Hydroxy-Modified MIL-53(Al) Structural Analogue by Lithium Doping, *Angew. Chem., Int. Ed.*, 2009, **48**, 4639–4642, DOI: 10.1002/anie.200806203.

5 P. García-Holley, B. Schweitzer, T. Islamoglu, Y. Liu, L. Lin, S. Rodriguez, M. H. Weston, J. T. Hupp, D. A. Gómez-Gualdrón, T. Yildirim and O. K. Farha, Benchmark Study of Hydrogen Storage in Metal–Organic Frameworks under Temperature and Pressure Swing Conditions, *ACS Energy Lett.*, 2018, **3**, 748–754, DOI: 10.1021/acsenergylett.8b00154.

6 M. Hartmann and M. Fischer, Amino-Functionalized Basic Catalysts with MIL-101 Structure, *Microporous Mesoporous Mater.*, 2012, **164**, 38–43, DOI: 10.1016/j.micromeso.2012.06.044.

7 P.-Z. Li, X.-J. Wang, J. Liu, J. S. Lim, R. Zou and Y. Zhao, A Triazole-Containing Metal-Organic Framework as a Highly Effective and Substrate Size-Dependent Catalyst for CO2 Conversion, *J. Am. Chem. Soc.*, 2016, **138**, 2142–2145, DOI: 10.1021/jacs.5b13335.

8 W. P. Lustig, S. Mukherjee, N. D. Rudd, A. V. Desai, J. Li and S. K. Ghosh, Metal–Organic Frameworks: Functional Luminescent and Photonic Materials for Sensing Applications, *Chem. Soc. Rev.*, 2017, **46**, 3242–3285, DOI: 10.1039/c6cs00930a.

9 P. Horcajada, R. Gref, T. Baati, P. K. Allan, G. Maurin, P. Couvreur, G. Férey, R. E. Morris and C. Serre, Metal–Organic Frameworks in Biomedicine, *Chem. Rev.*, 2012, **112**, 1232–1268, DOI: 10.1021/cr200256v.

10 H. Zheng, Y. Zhang, L. Liu, W. Wan, P. Guo, A. M. Nyström and X. Zou, One-Pot Synthesis of Metal-Organic Frameworks with Encapsulated Target Molecules and Their Applications for Controlled Drug Delivery, *J. Am. Chem. Soc.*, 2016, **138**, 962–968, DOI: 10.1021/jacs.5b11720.

11 P. Freund, I. Senkovska and S. Kaskel, Switchable Conductive MOF-Nanocarbon Composite Coatings as Threshold Sensing Architectures, *ACS Appl. Mater. Interfaces*, 2017, **9**, 43782–43789, DOI: 10.1021/acsami.7b13924.

12 A. K. Cheetham, G. Kieslich and H. H.-M. Yeung, Thermodynamic and Kinetic Effects in the Crystallization of Metal-Organic Frameworks, *Acc. Chem. Res.*, 2018, **51**, 659–667, DOI: 10.1021/acs.accounts.7b00497.

13 E. Stavitski, M. Goesten, J. Juan-Alcaniz, A. Martinez-Joaristi, P. Serra-Crespo, A. V. Petukhov, J. Gascon and F. Kapteijn, Kinetic Control of Metal-Organic Framework Crystallization Investigated by Time-Resolved in Situ X-Ray Scattering, *Angew. Chem., Int. Ed.*, 2011, **50**, 9624–9628, DOI: 10.1002/anie.201101757.

14 M. G. Goesten, P. C. M. M. Magusin, E. A. Pidko, B. Mezari, E. J. M. Hensen, F. Kapteijn and J. Gascon, Molecular Promoting of Aluminum Metal–Organic Framework Topology MIL-101 by *N,N*-Dimethylformamide, *Inorg. Chem.*, 2014, **53**, 882–887, DOI: 10.1021/ic402198a.

15 M. G. Goesten, E. Stavitski, J. Juan-Alcañiz, A. Martiñez-Joaristi, A. V. Petukhov, F. Kapteijn and J. Gascon, Small-Angle X-Ray Scattering Documents the Growth of Metal-Organic Frameworks, *Catal. Today*, 2013, **205**, 120–127, DOI: 10.1016/j.cattod.2012.08.044.

16 M. Haouas, C. Volkringer, T. Loiseau, G. Férey and F. Taulelle, In Situ NMR, ex Situ XRD and SEM Study of the Hydrothermal Crystallization of Nanoporous Aluminum Trimesates MIL-96, MIL-100, and MIL-110, *Chem. Mater.*, 2012, **24**, 2462–2471, DOI: 10.1021/cm300439e.

17 F. Carson, J. Su, A. E. Platero-Prats, W. Wan, Y. Yun, L. Samain and X. Zou, Framework Isomerism in Vanadium Metal–Organic Frameworks: MIL-88B(V) and MIL-101(V), *Cryst. Growth Des.*, 2013, **13**, 5036–5044, DOI: 10.1021/cg4012058.

18 T. Loiseau, C. Serre, C. Huguenard, G. Fink, F. Taulelle, M. Henry, T. Bataille and G. Férey, A Rationale for the Large Breathing of the Porous Aluminum Terephthalate (MIL-53) Upon Hydration, *Chem.–Eur. J.*, 2004, **10**, 1373–1382, DOI: 10.1002/chem.200305413.

19 G. Férey, Hybrid Porous Solids: Past, Present, Future, *Chem. Soc. Rev.*, 2008, **37**, 191–214, DOI: 10.1039/b618320b.

20 K. Barthelet, J. Marrot, G. Férey and D. Riou, A New Vanadocarboxylate with a Large Pore Hybrid Topology, *Chem. Commun.*, 2004, 520–521, DOI: 10.1039/b312589k.

21 C. Volkringer, M. Meddouri, T. Loiseau, N. Guillou, J. Marrot, G. Férey, M. Haouas, F. Taulelle, N. Audebrand and M. Latroche, The Kagomé Topology of the Gallium and Indium Metal-Organic Framework Types with a MIL-68 Structure: Synthesis, XRD, Solid-State NMR

Characterizations, and Hydrogen Adsorption, *Inorg. Chem.*, 2008, **47**, 11892–11901, DOI: 10.1021/ic801624v.

22 N. Stock and S. Biswas, Synthesis of Metal-Organic Frameworks (MOFs): Routes to Various MOF Topologies, Morphologies, and Composites, *Chem. Rev.*, 2012, **112**, 933–969, DOI: 10.1021/cr200304e.

23 Q. Yang, S. Vaesen, M. Vishnuvarthan, F. Ragon, C. Serre, A. Vimont, M. Daturi, G. de Weireld and G. Maurin, Probing the Adsorption Performance of the Hybrid Porous MIL-68(Al): A Synergic Combination of Experimental and Modelling Tools, *J. Mater. Chem.*, 2012, **22**, 10210, DOI: 10.1039/c2jm15609a.

24 A. Perea-Cachero, P. Calvo, E. Romero, C. Téllez and J. Coronas, Enhancement of Growth of MOF MIL-68(Al) Thin Films on Porous Alumina Tubes Using Different Linking Agents, *Eur. J. Inorg. Chem.*, 2017, 2532–2540, DOI: 10.1002/ejic.201700302.

25 A. Schneemann, V. Bon, I. Schwedler, I. Senkovska, S. Kaskel and R. A. Fischer, Flexible Metal–Organic Frameworks, *Chem. Soc. Rev.*, 2014, **43**, 6062–6096, DOI: 10.1039/c4cs00101j.

26 H. Reinsch, B. Marszałek, J. Wack, J. Senker, B. Gil and N. Stock, A New Al-MOF Based on a Unique Column-Shaped Inorganic Building Unit Exhibiting Strongly Hydrophilic Sorption Behaviour, *Chem. Commun.*, 2012, **48**, 9486, DOI: 10.1039/c2cc34909d.

27 N. Stock, in *Encyclopedia of Inorganic and Bioinorganic Chemistry*, ed. R. A. Scott, John Wiley & Sons, Ltd, Chichester, UK, 2011, pp. 1–16.

28 H. Embrechts, M. Kriesten, K. Hoffmann, W. Peukert, M. Hartmann and M. Distaso, Elucidation of the Formation Mechanism of Metal-Organic Frameworks *via* in-Situ Raman and FTIR Spectroscopy under Solvothermal Conditions, *J. Phys. Chem. C*, 2018, **122**, 12267–12278.

29 Z. Li, Y. Wu, J. Li, Y. Zhang, X. Zou and F. Li, The Metal-Organic Framework MIL-53(Al) Constructed from Multiple Metal Sources: Alumina, Aluminum hydroxide, and Boehmite, *Chem.–Eur. J.*, 2015, **21**, 6913–6920, DOI: 10.1002/chem.201406531.

30 M. Sánchez-Sánchez, N. Getachew, K. Díaz, M. Díaz-García, Y. Chebude and I. Díaz, Synthesis of Metal–Organic Frameworks in Water at Room Temperature: Salts as Linker Sources, *Green Chem.*, 2015, **17**, 1500–1509, DOI: 10.1039/c4gc01861c.

31 S. Kaskel, *Chemistry of Metal-Organic Frameworks*, Wiley - VCH Verlag GmbH & Co, Weinheim, 2016.

32 M. Kriesten, K. Hoffmann and M. Hartmann, Comment on "Insight Into the Reversible Structural Crystalline-State Transformation from MIL-53(Al) to MIL-68(Al)", *CrystEngComm*, 2018, **20**, 3117–3119, DOI: 10.1039/C8CE00398J.

33 L. Wu, W. Wang, R. Liu, G. Wu and H. Chen, Impact of the functionalization onto structure transformation and gas adsorption of MIL-68(In), *R. Soc. Open Sci.*, 2018, **5**, 181378, DOI: 10.1098/rsos.181378.

34 T. Tsuruoka, S. Furukawa, Y. Takashima, K. Yoshida, S. Isoda and S. Kitagawa, Nanoporous Nanorods

Fabricated by Coordination Modulation and Oriented Attachment Growth, *Angew. Chem., Int. Ed.*, 2009, **48**, 4739–4743, DOI: 10.1002/anie.200901177.

35 S. Diring, S. Furukawa, Y. Takashima, T. Tsuruoka and S. Kitagawa, Controlled Multiscale Synthesis of Porous Coordination Polymer in Nano/Micro Regimes, *Chem. Mater.*, 2010, **22**, 4531–4538, DOI: 10.1021/cm101778g.

36 Z. Hu, I. Castano, S. Wang, Y. Wang, Y. Peng, Y. Qian, C. Chi, X. Wang and D. Zhao, Modulator Effects on the Water-Based Synthesis of Zr/Hf Metal–Organic Frameworks: Quantitative Relationship Studies between Modulator, Synthetic Condition, and Performance, *Cryst. Growth Des.*, 2016, **16**, 2295–2301, DOI: 10.1021/acs.cgd.6b00076.

37 J. Ren, N. M. Musyoka, H. W. Langmi, T. Segakweng, B. C. North, M. Mathe and X. Kang, Modulated Synthesis of Chromium-Based Metal-Organic Framework (MIL-101) with Enhanced Hydrogen Uptake, *Int. J. Hydrogen Energy*, 2014, **39**, 12018–12023, DOI: 10.1016/j.ijhydene.2014.06.019.

38 A. Schaate, P. Roy, A. Godt, J. Lippke, F. Waltz, M. Wiebcke and P. Behrens, Modulated Synthesis of Zr-Based Metal-Organic Frameworks: From Nano to Single Crystals, *Chem.–Eur. J.*, 2011, **17**, 6643–6651, DOI: 10.1002/chem.201003211.

39 G. Zahn, P. Zerner, J. Lippke, F. L. Kempf, S. Lilienthal, C. A. Schröder, A. M. Schneider and P. Behrens, Insight into the Mechanism of Modulated Syntheses: in Situ Synchrotron Diffraction Studies on the Formation of Zr-Fumarate MOF, *CrystEngComm*, 2014, **16**, 9198–9207, DOI: 10.1039/c4ce01095g.

40 J. M. Chin, E. Y. Chen, A. G. Menon, H. Y. Tan, A. T. S. Hor, M. K. Schreyer and J. Xu, Tuning the Aspect Ratio of NH2-MIL-53(Al) Microneedles and Nanorods *via* Coordination Modulation, *CrystEngComm*, 2013, **15**, 654–657, DOI: 10.1039/C2CE26586A.

41 G. N. R. Tripathi and S. J. Sheng, Solid-state vibrational spectra and structures of terephtalic acid and the terephtalate ion, *J. Mol. Struct.*, 1979, **57**, 21–34.

42 A. E. J. Hoffman, L. Vanduyfhuys, I. Nevjestić, J. Wieme, S. M. J. Rogge, H. Depauw, P. van der Voort, H. Vrielinck and V. van Speybroeck, Elucidating the Vibrational Fingerprint of the Flexible Metal-Organic Framework MIL-53(Al) Using a Combined Experimental/Computational Approach, *J. Phys. Chem. C*, 2018, **122**, 2734–2746, DOI: 10.1021/acs.jpcc.7b11031.

43 F. Rouquerol, J. Rouquerol and K. Sing, *Adsorption by Powders and Porous Solids. Principles, Methodology and Applications*, Academic Press, San Diego, 1999.

44 T. Loiseau, C. Volkringer, M. Haouas, F. Taulelle and G. Férey, Crystal Chemistry of Aluminium Carboxylates: From Molecular Species Towards Porous Infinite Three-Dimensional Networks, *C. R. Chim.*, 2015, **18**, 1350–1369, DOI: 10.1016/j.crci.2015.08.006.

45 R. Lundblad and F. Macdonald, *Handbook of Biochemistry and Molecular Biology*, CRC Press, Boca Raton, Fla, 4th edn, 2010.

46 N. M. D. Brown, R. B. Floyd and D. G. Walmsley, Inelastic Electron Tunnelling Spectroscopy (IETS) of Carboxylic

Acids and Related Systems Chemisorbed on Plasma-Grown Aluminium Oxide, *J. Chem. Soc., Faraday Trans.*, 1979, **75**, 17–31, DOI: 10.1039/F29797500017.

47 A. Gavezzotti, Hydrogen Bond Strength and Bond Geometry in Cyclic Dimers of Crystalline Carboxylic Acids, *Acta Crystallogr., Sect. B: Struct. Sci.*, 2008, **64**, 401–403, DOI: 10.1107/S0108768108007556.

48 U. Lourderaj, K. Giri and N. Sathyamurthy, Ground and Excited States of the Monomer and Dimer of Certain Carboxylic Acids, *J. Phys. Chem. A*, 2006, **110**, 2709–2717, DOI: 10.1021/jp056491x.

49 E. J. P. Feijen, J. A. Martens and P. A. Jacobs, Zeolites and their Mechanism of Synthesis, *Stud. Surf. Sci. Catal.*, **84**, 3–21, DOI: 10.1016/S0167-2991(08)64074-4.

50 G. Öhlmann, H. Pfeifer and R. Fricke, *Catalysis and Adsorption by Zeolites*, Elsevier, Burlington, 1991.